

LETTER TO THE EDITOR

On binary driven hypernovae and their nested late X-ray emission

R. Ruffini^{1,2,3,4}, M. Muccino^{1,2}, C. L. Bianco^{1,2}, M. Enderli^{1,3}, L. Izzo^{1,2}, M. Kovacevic^{1,3}, A. V. Penacchioni⁴,
G. B. Pisani^{1,3}, J. A. Rueda^{1,2,4}, Y. Wang^{1,2}

¹ Dip. di Fisica and ICRA, Sapienza Università di Roma, Piazzale Aldo Moro 5, I-00185 Rome, Italy,

² ICRA Net, Piazza della Repubblica 10, I-65122 Pescara, Italy,

³ Université de Nice Sophia Antipolis, CEDEX 2, Grand Château Parc Valrose, Nice, France,

⁴ ICRA Net-Rio, Centro Brasileiro de Pesquisas Físicas, Rua Dr. Xavier Sigaud 150, Rio de Janeiro, RJ, 22290-180, Brazil.

ABSTRACT

Context. The induced gravitational collapse (IGC) paradigm addresses the very energetic (10^{52} – 10^{54} erg) long gamma-ray bursts (GRBs) associated to supernovae (SNe). Unlike the traditional “collapsar” model, an evolved FeCO core with a companion neutron star (NS) in a tight binary system is considered as the progenitor. This special class of sources, here named “binary driven hypernovae” (BdHNe), presents a composite sequence composed of four different episodes with precise spectral and luminosity features.

Aims. We first compare and contrast the steep decay, the plateau, and the power-law decay of the X-ray luminosities of three selected BdHNe (GRB 060729, GRB 061121, and GRB 130427A). Second, to explain the different sizes and Lorentz factors of the emitting regions of the four episodes, for definiteness, we use the most complete set of data of GRB 090618. Finally, we show the possible role of r-process, which originates in the binary system of the progenitor.

Methods. We compare and contrast the late X-ray luminosity of the above three BdHNe. We examine correlations between the time at the starting point of the constant late power-law decay t_a^* , the average prompt luminosity $\langle L_{iso} \rangle$, and the luminosity at the end of the plateau L_a . We analyze a thermal emission (~ 0.97 – 0.29 keV), observed during the X-ray steep decay phase of GRB 090618.

Results. The late X-ray luminosities of the three BdHNe, in the rest-frame energy band 0.3–10 keV, show a precisely constrained “nested” structure. In a space-time diagram, we illustrate the different sizes and Lorentz factors of the emitting regions of the three episodes. For GRB 090618, we infer an initial dimension of the thermal emitter of $\sim 7 \times 10^{12}$ cm, expanding at $\Gamma \approx 2$. We find tighter correlations than the Dainotti-Willingale ones.

Conclusions. We confirm a constant slope power-law behavior for the late X-ray luminosity in the source rest frame, which may lead to a new distance indicator for BdHNe. These results, as well as the emitter size and Lorentz factor, appear to be inconsistent with the traditional afterglow model based on synchrotron emission from an ultra-relativistic ($\Gamma \sim 10^2$ – 10^3) collimated jet outflow. We argue, instead, for the possible role of r-process, originating in the binary system, to power the mildly relativistic X-ray source.

Key words. supernovae: general — binaries: general — gamma-ray burst: general — black hole physics — nuclear reactions, nucleosynthesis, abundances — stars: neutron

1. Introduction

The induced gravitational collapse (IGC) paradigm has been widely illustrated (Ruffini et al., 2006, 2007, 2008; Rueda & Ruffini, 2012; Izzo et al., 2012a). It assumes that long, energetic (10^{52} – 10^{54} erg) gamma-ray bursts (GRBs) associated to supernovae (SNe) originate in a close binary system composed of an evolved massive star (likely a FeCO core) in the latest phases of its thermonuclear evolution and a neutron star (NS) companion. From an observational point of view, the complete time sequence of the IGC paradigm binary system has been identified in GRB 090618 (Izzo et al., 2012b), GRB 101023 (Penacchioni et al., 2012), GRB 110907B (Penacchioni et al., 2013), and GRB 970828 (Ruffini et al., 2013). We name these especially energetic systems, here, fulfilling the IGC paradigm, “binary driven hypernovae” (BdHNe), to differentiate them from the traditional less energetic hypernovae.

In this Letter we introduce the IGC paradigm space-time diagram for the four distinct emission episodes (see Fig. 1):

Episode 1 corresponds to the onset of the FeCO core SN explosion, creating a new-NS (ν -NS, see A). Part of the SN ejecta triggers an accretion process onto the NS companion (see Rueda

& Ruffini, 2012; Izzo et al., 2012a, and B in Fig. 1), and a prolonged interaction between the ν -NS and the NS binary companion occurs (C). This leads to a spectrum with an expanding thermal component plus an extra power law (see Fig. 16 in Izzo et al., 2012b, and Fig. 4 in Ruffini et al., 2013).

Episode 2 occurs when the companion NS reaches its critical mass and collapses to a black hole (BH), emitting the GRB (D) with Lorentz factors $\Gamma \approx 10^2$ – 10^3 (for details, see e.g. Ruffini et al., 2010; Izzo et al., 2012b; Ruffini et al., 2013).

Episode 3, observed in the X-rays, shows very precise behavior consisting of a steep decay, starting at the end point of the prompt emission (see E), and then a plateau phase, followed by a late constant power-law decay (see, e.g., Izzo et al., 2012b; Penacchioni et al., 2012; Ruffini et al., 2013).

Episode 4, not shown in Fig. 1, corresponds to the optical SN emission due to the ^{56}Ni decay (see Arnett, 1996) occurring after ~ 10 – 15 days in the cosmological rest frame. In all BdHNe, the SN appears to have the same luminosity as in the case of SN 1998bw (Amati et al., 2007). Although the presence of the SN is implicit in all the sources fulfilling the IGC paradigm, it is only detectable for GRBs at $z \lesssim 1$, in view of the limitations of the current optical telescopes.

Send offprint requests to: e-mail: marco.muccino@icra.it

arXiv:1404.3946v2 [astro-ph.HE] 14 May 2014

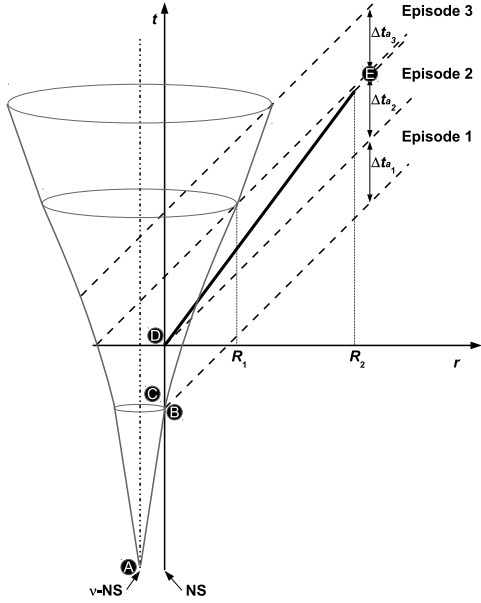


Fig. 1. IGC space-time diagram (not in scale) illustrates the relativistic motion of Episode 2 ($\Gamma \approx 500$, thick line) and the non-relativistic Episode 1 ($\Gamma \approx 1$) and Episode 3 ($\Gamma \approx 2$). Emissions from different radii, R_1 ($\sim 10^{13}$ cm) and R_2 ($\sim 10^{16}$ – 10^{17} cm), contribute to the transition point (E). Clearly, the X-ray luminosity originates in the SN remnant or in the newly-born BH, but not in the GRB.

We are going to see in this Letter that Episodes 1 and 2 can differ greatly in luminosity and timescale from source to source, while we confirm that in Episode 3, the late X-ray luminosities overlap: they follow a common power-law behavior with a constant slope in the source rest frame (Pisani et al., 2013). We point out here that the starting point of this power-law component is a function of the GRB isotropic energy E_{iso} .

The main goals of this Letter consist in a) comparing and contrasting the steep decay, the plateau, and the power-law decay of the X-ray luminosities as functions of E_{iso} by considering three selected GRBs (060729, 061121, and 130427A); b) pointing out the difference in the size and the Lorentz factors of the emitting regions of Episodes 1, 2, and 3 (for definiteness we use as prototype the source with the most complete dataset, GRB 090618); c) drawing attention to the possible role of the r-process, originating in the binary system of the progenitor, to power the mildly relativistic X-ray emission in the late phases of Episode 3.

2. The case of GRB 090618

We illustrate the difference in the emitting region sizes in the three episodes and their corresponding Lorentz factors:

Episode 1 has a thermal component expanding from $\sim 10^9$ cm to $\sim 10^{10}$ cm on a rest-frame timescale of ~ 30 s with an average velocity of $\sim 4 \times 10^8$ cm s^{-1} (see Izzo et al., 2012b). The total energy is 4.1×10^{52} erg, well above the traditional kinetic energy expected in the early phases of a SN, and it originates in the accretion of the material of the SN ejecta on the companion NS in the binary system (Rueda & Ruffini, 2012; Ruffini et al., 2013).

Episode 2 has been shown to be the ultra-relativistic prompt emission episode (e.g., the actual GRB) stemming from the collapse of the NS to a BH. Its isotropic energy is 2.5×10^{53} erg. The

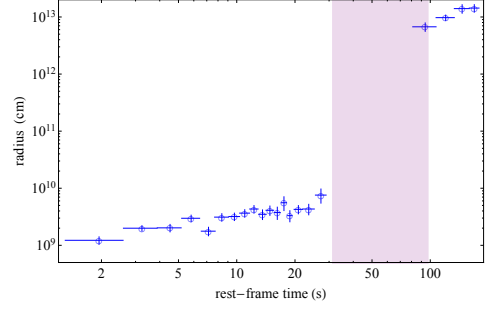


Fig. 2. Radii (open blue circles) of the emitting regions, measured in the cosmological rest frame. Episode 1 radius ranges from $\sim 10^9$ cm to $\sim 10^{10}$ and expands at $\Gamma \approx 1$ (Izzo et al., 2012b). The Episode 3 radius, in the early phases of the steep decay, starts from a value of $\sim 7 \times 10^{12}$ cm and expands at $\Gamma \approx 2$. The Episode 2 rest-frame duration is indicated by the shaded purple region. The expansion velocity at late times is expected to approach the asymptotic value of $0.1c$ observed in the optical spectra (Della Valle, 2011), in the absence of any further acceleration process.

characteristic Lorentz factor at the transparency of the fireshell has been found to be $\Gamma = 490$ for GRB 090618. The characteristic spatial extension goes all the way up to $\sim 10^{16}$ – 10^{17} cm, reached at the end of Episode 2 (see Fig. 10 in Izzo et al., 2012b). **Episode 3** has an isotropic energy of $\approx 6 \times 10^{51}$ erg. A striking feature occurs during its steep decay phase: in the early observed 150 s, Page et al. (2011) have found a thermal component with a decreasing temperature from ~ 0.97 keV to ~ 0.29 keV (see also Starling et al., 2012). The surface radius of the emitter can be inferred from the observed temperature T_o and flux F_{BB} of the thermal component. We have, in fact (Izzo et al., 2012b),

$$r \approx \Gamma d_l (1+z)^{-2} \sqrt{F_{BB}/(\sigma T_o^4)}, \quad (1)$$

where d_l is the luminosity distance in the Λ CDM cosmological model and σ the Stefan-Boltzmann constant. As usual, $\Gamma = 1/\sqrt{1-\beta^2}$, where $\beta = v/c$ is the expansion velocity in units of the speed of light c .

In parallel, the relation between the detector arrival time t_a^d , the cosmological rest-frame arrival time t_a and the laboratory time t , is given by $t_a^d \equiv t_a(1+z) = t(1-\beta \cos \theta)(1+z)$, where θ is the displacement angle of the considered photon emission point from the line of sight (see, e.g., Bianco et al., 2001). We can then deduce the expansion velocity β , assumed to be constant, from the ratio between the variation of the emitter radius Δr and the emission duration in laboratory frame Δt , i.e. $\beta = \Delta r/(c\Delta t)$. Using the condition $\beta \leq \cos \theta \leq 1$ (Bianco et al., 2001), we obtain $0.75 \leq \beta \leq 0.89$ and, correspondingly, $1.50 \leq \Gamma \leq 2.19$ and radii $r \sim 10^{13}$ cm (see Fig. 2).

As is clear from Fig. 1, a sharp transition occurs between the end of Episode 2, where the characteristic dimensions reached by the GRB are $\sim 10^{16}$ – 10^{17} cm, and the emission at the beginning of X-ray luminosity, with an initial size of $\sim 7 \times 10^{12}$ cm. This leads to the conclusion that the X-ray emission of Episode 3 originates in the SN ejecta or in the accretion on the newly born BH and, anyway, not from the GRB.

3. The “nested” structure of Episode 3

We now turn to show the “nested” structure of the late X-ray luminosity. Pisani et al. (2013) have shown that the X-ray rest-

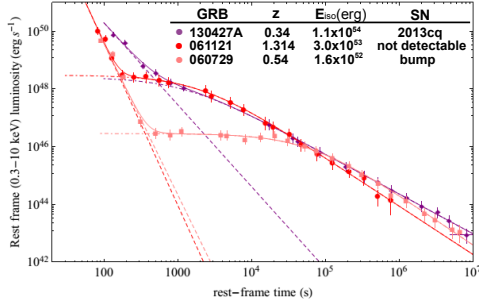


Fig. 3. Rest-frame 0.3–10 keV re-binned luminosity light curves of GRB 130427A (purple), GRB 061121 (red, shifted by 50s in rest frame), and GRB 060729 (pink). The light curves are fitted by using a power-law for the steep decay phase (dashed lines) and the function in Eq. (2) for the plateau and the late decay phases (dot-dashed curves).

frame 0.3–10 keV luminosity light curves present a constant decreasing power-law behavior, at $t_a \gtrsim 10^4$ s, with typical slopes of $-1.7 \lesssim \alpha_X \lesssim -1.3$. This has been proven in a sample of six BdHNe: GRBs 060729, 061007, 080319B, 090618, 091127, and 111228, hereafter *golden sample* (GS, see, e.g., Izzo et al., 2013; Pisani et al., 2013). That the late X-ray emission could play a fundamental role as a distance indicator has been explored inferring the redshifts of GRBs 101023 and 110709B (Penacchioni et al., 2012, 2013). The IGC paradigm also allowed predicting ~ 10 –15 days in the cosmological rest frame before its discovery, the occurrence of the SN associated to GRB 130427A, the most luminous source ever observed in γ rays with $E_{iso} \approx 10^{54}$ erg and $z = 0.34$ (Xu et al., 2013b; Flores et al., 2013). This was later confirmed by the observations (de Ugarte Postigo et al., 2013; Levan et al., 2013; Watson et al., 2013; Xu et al., 2013a).

We compare and contrast GRB 130427A X-ray data with GRB 060729, a member of the GS, and GRB 061121, which shows the general behavior of BdHNe. GRB 060729, at $z = 0.54$, has $E_{iso} = 1.6 \times 10^{52}$ erg (Grupe et al., 2007) and a SN bump in its optical afterglow (Cano et al., 2011). GRB 061121, at $z = 1.314$ (Bloom et al., 2006), has $E_{iso} = 3.0 \times 10^{53}$ erg, and its Episode 4 is clearly missing in view of the high cosmological redshift.

In Fig. 3 we have plotted the rebinned rest-frame 0.3–10 keV luminosity light curves of GRBs 130427A, 060729, and 061121. Their steep decay is modeled by a power-law function, i.e. $L_p(t_a/100)^{-\alpha_p}$, where L_p and α_p are the power-law parameters. The plateau and the late power-law decay are instead modeled by using the following phenomenological function

$$L(t_a) = L_X(1 + t_a/\tau)^{\alpha_X}, \quad (2)$$

where L_X , α_X , and τ , respectively, are the plateau luminosity, the late power-law decay index, and the characteristic timescale of the end of the plateau. From Eq. (2), we have defined the end of the plateau at the rest-frame time $t_a^* = \tau[(1/2)^{1/\alpha_X} - 1]$, when the luminosity of the plateau is half of the initial one, $L_a(t_a^*) = L_X/2$.

From this fitting procedure, we can conclude that the three BdHN systems considered here share the following properties:

- a)** the power-law decay for the more energetic sources starts directly from the steep decay, well before the $t_a \approx 2 \times 10^4$ s, as indicated in Pisani et al. (2013). Consequently, the plateau shrinks as a function of the increasing E_{iso} (see Fig. 3);
- b)** the luminosities in the power-law decay are uniquely functions of the cosmological rest-frame arrival time t_a independently on the E_{iso} of each source (see Fig. 3);

Table 1. List of the quantities of the considered sources and best fit parameters of the correlations in Fig. 4.

GRB	$\langle L_{iso} \rangle$ (10^{50} erg/s)	t_a^* (ks)	L_a (10^{47} erg/s)
060729	1.25 ± 0.08	27.4 ± 1.4	0.20 ± 0.01
061007	267 ± 18	0.041 ± 0.036	$521 \pm \text{unc}$
080319B	279 ± 7	0.12 ± 0.03	430 ± 170
090618	34.7 ± 0.3	0.74 ± 0.03	7.81 ± 0.17
091127	26.8 ± 0.3	1.31 ± 0.10	4.39 ± 0.26
111228A	4.79 ± 0.24	2.17 ± 0.27	1.38 ± 0.10
130427A	98 ± 15	0.16 ± 0.03	121 ± 21
Correlation	m_i	q_i	σ_i
$\langle L_{iso} \rangle - t_a^*$	$-(0.90 \pm 0.09)$	54.0 ± 0.3	0.20 ± 0.05
$L_a - t_a^*$	$-(1.34 \pm 0.14)$	52.0 ± 0.4	0.26 ± 0.08

c) most remarkably, the overlapping of the X-ray light curves reveals a “nested” structure of BdHN Episodes 3.

In our sample of BdHNe, we verify the applicability of the Dainotti-Willingale relations $\langle L_{iso} \rangle - t_a^*$ and $L_a - t_a^*$ (Dainotti et al., 2008, 2011b; Willingale et al., 2007), where $\langle L_{iso} \rangle = E_{iso}/t_{a,90}$ is the averaged luminosity of the prompt and $t_{a,90}$ is the rest-frame t_{90} duration of the burst. The resulting correlations, $\log_{10} Y_i = m_i \log_{10} X_i + q_i$, are shown in Fig. 4. The parameters of each BdHN and the best fit parameters, m_i and q_i (where $i = 1, 2$), are summarized in Table 1. As is clear from the extra scatter values σ_i , our total BdHN sample provides tighter correlations. The extra scatter of the $L_a - t_a^*$, $\sigma = 0.26$, is less than the Dainotti et al. (2011a) ones, i.e., $\sigma = 0.76$ for the whole sample of 62 bursts and $\sigma = 0.40$ for the best subsample of eight bursts (U0095). The Dainotti-Willingale correlations consider X-ray afterglows characterized by a steep decay, a plateau phase, and a late power-law decay (Nousek et al., 2006; Zhang et al., 2006), independently of their energetics. In our BdHN sample we limit the attention to a) the most energetic sources, 10^{52} – 10^{54} erg, b) the presence of four emission episodes (neglecting Episode 4 for $z > 1$), and c) sources with determined redshift and complete data at $t_a = 10^4$ – 10^6 s. All these conditions appear to be necessary to fulfill the nested structure in Fig. 3 and the tighter correlations between the astrophysical parameters $\langle L_{iso} \rangle$, L_a , and t_a^* in Fig. 4.

To explain the above nested power-law decay and constrained correlations, we consider the decay of heavy elements produced in the r-process as a viable energy source (Burbidge et al., 1957), originating in binary NS mergers (see, e.g., Li & Paczyński, 1998; Janka et al., 1999; Rosswog et al., 2004; Oechslin et al., 2007; Goriely et al., 2011; Piran et al., 2014).

Li & Paczyński (1998) have shown that the emission from the surface of an optically thick expanding ejecta in an adiabatic regime provides a flat light curve (see also Arnett, 1982). This can explain, in principle, the observed steep decay and plateau phase of Episode 3 (see Fig. 3). After the ejecta becomes transparent, the heating source term due to the nuclear decays of the heavy nuclei, generated via r-process, becomes directly observable and dominates. The avalanche of decays with different lifetimes then provides the total energy release per unit mass per time that follows a power-law distribution, whose decay index has been estimated to be $-1.4 \lesssim \alpha \lesssim -1.1$ (Metzger et al., 2010). These values are strikingly similar to the ones we have found in the late X-ray luminosity.

This power-law behavior is different from the exponential decay observed in the optical light curves of traditional SN, powered by the decay of a single element ($^{56}\text{Ni} \rightarrow ^{56}\text{Co} \rightarrow ^{56}\text{Fe}$), which is not produced in the avalanche of many decays as in the r-process.

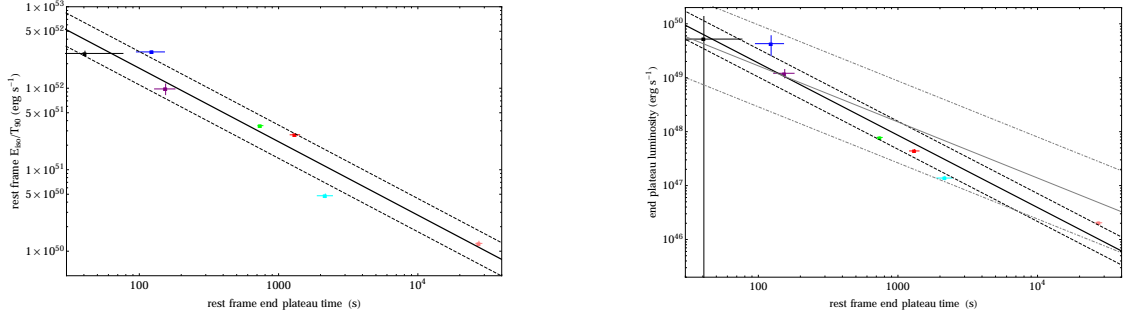


Fig. 4. The $\langle L_{iso} \rangle - t_a^*$ (left) and the $L_a - t_a^*$ (right) correlations (solid black lines) and the corresponding 1σ confidence levels (dashed black lines). The considered sources are GRB 060729 (pink), GRB 061007 (black), GRB 080319B (blue), GRB 090618 (green), GRB 091127 (red), GRB 111228A (cyan), and GRB 130427A (purple). The tigher BdHNe $L_a - t_a^*$ correlation is compared to the one in Dainotti et al. (2011a), corresponding to $m = -1.04$ and $q = 51.30$ (solid gray line) and $\sigma = 0.76$ (dotted-dashed gray lines).

4. Conclusions

To summarize, short GRBs have been shown to come from binary NS mergers (see, e.g., Goodman, 1986; Paczynski, 1986; Eichler et al., 1989; Meszaros & Rees, 1997; Rosswog et al., 2003; Lee et al., 2004; and more recently Muccino et al., 2013). Our subclass of long, extremely energetic (10^{52} – 10^{54} erg) sources is also initially driven by a tight binary system, formed by a ν -NS and a companion NS, surrounded by the SN ejecta (see Fig. 1). Then we denoted these most energetic GRBs by “BdHNe”. This is clearly different from the gravitational collapse of a single massive progenitor star described by the collapsar model (Woosley, 1993; MacFadyen & Woosley, 1999; Woosley & Bloom, 2006).

We compared and contrasted the late X-ray luminosities of three BdHNe with different E_{iso} , finding a nested structure. We showed tight correlations between $\langle L_{iso} \rangle$, L_a and t_a^* (see Fig. 4 and Table 1) in agreement with the Dainotti-Willingale ones.

The above scaling laws, the nesting, and the initial dimension of $\sim 7 \times 10^{12}$ cm and Lorentz factor of $\Gamma \approx 2$ obtained from the steep decay of the X-ray luminosity put stringent limits on alternative theoretical models. They do not appear to be explainable within the traditional fireball jetted model, originating in the synchrotron radiation emitted by a decelerating relativistic shell with $\Gamma \sim 10^2$ and colliding with the circumburst medium at distances $\sim 10^{16}$ cm (see, e.g., Sari et al., 1998; Piran, 2005; Meszaros, 2006; Gehrels et al., 2009, and reference therein). In this Letter we alternatively proposed that the late X-ray luminosity comes from the wide angle emission of the SN ejecta or in the accretion on the newly born BH. We call the attention on the role of the energy release in the SN ejecta from the decay of very heavy nuclei generated by r-process in binary NSs (Li & Paczyński, 1998). This heavy nuclei avalanche decay (see, e.g., Metzger et al., 2010) may well explain the late X-ray luminosity of Episode 3. This emission follows the steep decay and plateau phase of the adiabatic optically thick expansion, prior to reaching transparency (see Fig. 3).

In the case of binary systems with longer periods and/or a lower accretion rate, which do not allow the NS companion to reach its critical mass and to form a BH, Episode 2 is missing. The presence of the companion NS will nevertheless strip the H and He envelopes of the core progenitor star. These sources have low energetic bursts ($E_{iso} < 10^{52}$ erg), such as GRB 060218 and GRB 980425, and their X-ray luminosity light curves do not overlap with the ones of our more energetic sample of BdHNe.

These systems do not conform to the IGC paradigm and are traditional hypernovae¹.

Acknowledgements. This work made use of data supplied by the UK Swift Science Data Center at the University of Leicester. ME, MK, and GBP are supported by the Erasmus Mundus Joint Doctorate Program by grant Nos. 2012-1710, 2013-1471, and 2011-1640, respectively, from the EACEA of the European Commission. We warmly thank the anonymous referee for very constructive suggestions that improved the presentation of this Letter.

References

- Amati, L., Della Valle, M., Frontera, F., et al. 2007, *A&A*, 463, 913
 Arnett, D. 1996, *Space Sci. Rev.*, 78, 559
 Arnett, W. D. 1982, *ApJ*, 253, 785
 Bianco, C. L., Ruffini, R., & Xue, S.-S. 2001, *A&A*, 368, 377
 Bloom, J. S., Perley, D. A., & Chen, H. W. 2006, *GCN Circ.*, 5826
 Burbidge, E. M., Burbidge, G. R., Fowler, W. A., & Hoyle, F. 1957, *Reviews of Modern Physics*, 29, 547
 Cano, Z., Bersier, D., Guidorzi, C., et al. 2011, *MNRAS*, 174
 Dainotti, M. G., Cardone, V. F., & Capozziello, S. 2008, *MNRAS*, 391, L79
 Dainotti, M. G., Fabrizio Cardone, V., Capozziello, S., Ostrowski, M., & Willingale, R. 2011a, *ApJ*, 730, 135
 Dainotti, M. G., Ostrowski, M., & Willingale, R. 2011b, *MNRAS*, 418, 2202
 de Ugarte Postigo, A., Xu, D., Leloudas, G., et al. 2013, *GCN Circ.*, 14646, 1
 Della Valle, M. 2011, *International Journal of Modern Physics D*, 20, 1745
 Eichler, D., Livio, M., Piran, T., & Schramm, D. N. 1989, *Nature*, 340, 126
 Flores, H., Covino, S., Xu, D., et al. 2013, *GCN Circ.*, 14491, 1
 Gehrels, N., Ramirez-Ruiz, E., & Fox, D. B. 2009, *ARA&A*, 47, 567
 Goodman, J. 1986, *ApJ*, 308, L47
 Goriely, S., Bauswein, A., & Janka, H.-T. 2011, *ApJ*, 738, L32
 Grupe, D., Gronwall, C., Wang, X.-Y., et al. 2007, *ApJ*, 662, 443
 Izzo, L., Pisani, G. B., Muccino, M., et al. 2013, *EAS Publ. Ser.*, 61, 595
 Izzo, L., Rueda, J. A., & Ruffini, R. 2012a, *A&A*, 548, L5
 Izzo, L., Ruffini, R., Penacchioni, A. V., et al. 2012b, *A&A*, 543, A10
 Janka, H.-T., Eberl, T., Ruffert, M., & Fryer, C. L. 1999, *ApJ*, 527, L39
 Lee, W. H., Ramirez-Ruiz, E., & Page, D. 2004, *ApJ*, 608, L5
 Levan, A. J., Fruchter, A. S., Graham, J., et al. 2013, *GCN Circ.*, 14686, 1
 Li, L.-X. & Paczyński, B. 1998, *ApJ*, 507, L59
 MacFadyen, A. I. & Woosley, S. E. 1999, *ApJ*, 524, 262
 Meszaros, P. 2006, *Reports on Progress in Physics*, 69, 2259
 Meszaros, P. & Rees, M. J. 1997, *ApJ*, 482, L29
 Metzger, B. D., Martínez-Pinedo, G., Darbha, S., et al. 2010, *MNRAS*, 406, 2650
 Muccino, M., Ruffini, R., Bianco, C. L., Izzo, L., & Penacchioni, A. V. 2013, *ApJ*, 763, 125
 Nousek, J. A., Kouveliotou, C., Grupe, D., et al. 2006, *ApJ*, 642, 389
 Oechslin, R., Janka, H.-T., & Marek, A. 2007, *A&A*, 467, 395
 Paczynski, B. 1986, *ApJ*, 308, L43
 Page, K. L., Starling, R. L. C., Fitzpatrick, G., et al. 2011, *MNRAS*, 416, 2078
 Penacchioni, A. V., Ruffini, R., Bianco, C. L., et al. 2013, *A&A*, 551, A133
 Penacchioni, A. V., Ruffini, R., Izzo, L., et al. 2012, *A&A*, 538, A58
 Piran, T. 2005, *Rev. Mod. Phys.*, 76, 1143

¹ <http://nsm.utdallas.edu/texas2013/proceedings/3/1/Ruffini.pdf>

- Piran, T., Korobkin, O., & Rosswog, S. 2014, arXiv:1401.2166
- Pisani, G. B., Izzo, L., Ruffini, R., et al. 2013, *A&A*, 552, L5
- Rosswog, S., Ramirez-Ruiz, E., & Davies, M. B. 2003, *MNRAS*, 345, 1077
- Rosswog, S., Speith, R., & Wynn, G. A. 2004, *MNRAS*, 351, 1121
- Rueda, J. A. & Ruffini, R. 2012, *ApJ*, 758, L7
- Ruffini, R., Bernardini, M. G., Bianco, C. L., et al. 2008, in *The Eleventh Marcel Grossmann Meeting*, ed. H. Kleinert, R. T. Jantzen, & R. Ruffini (Singapore: World Scientific), 368–505
- Ruffini, R., Bernardini, M. G., Bianco, C. L., et al. 2007, *ESA SP*, 622, 561
- Ruffini, R., Bernardini, M. G., Bianco, C. L., et al. 2006, in *The Tenth Marcel Grossmann Meeting.*, ed. M. Novello, S. Perez Bergliaffa, & R. Ruffini (Singapore: World Scientific), 369
- Ruffini, R., Izzo, L., Muccino, M., et al. 2013, arXiv:1311.7432
- Ruffini, R., Vereshchagin, G., & Xue, S.-S. 2010, *Phys. Rep.*, 487, 1
- Sari, R., Piran, T., & Narayan, R. 1998, *ApJ*, 497, L17
- Starling, R. L. C., Page, K. L., Pe’Er, A., Beardmore, A. P., & Osborne, J. P. 2012, *MNRAS*, 427, 2950
- Watson, A. M., Butler, N., Kutyrev, A., et al. 2013, *GCN Circ.*, 14666, 1
- Willingale, R., O’Brien, P. T., Osborne, J. P., et al. 2007, *ApJ*, 662, 1093
- Woosley, S. E. 1993, *ApJ*, 405, 273
- Woosley, S. E. & Bloom, J. S. 2006, *ARAA*, 44, 507
- Xu, D., de Ugarte Postigo, A., Kruehler, T., et al. 2013a, *GCN Circ.*, 14597, 1
- Xu, D., de Ugarte Postigo, A., Schulze, S., et al. 2013b, *GCN Circ.*, 14478, 1
- Zhang, B., Fan, Y. Z., Dyks, J., et al. 2006, *ApJ*, 642, 354